Geospatial Health 3(2), 2009, pp. 157-176

Developing operational algorithms using linear and non-linear squares estimation in Python® for the identification of *Culex pipiens* and *Culex restuans* in a mosquito abatement district (Cook County, Illinois, USA)

Benjamin G. Jacob, Weidong Gu, Erik X. Caamano, Robert J. Novak

Department of Medicine, William C. Gorgas Center for Geographic Medicine, University of Alabama, 845 19th Street South, Birmingham, AL, 35294, USA

Abstract. In this research, community level spatial models were developed for determining mosquito abundance and environmental factors that could aid in the risk prediction of West Nile virus (WNv) outbreaks. Adult *Culex pipiens* and *Culex restuan* mosquitoes and multiple habitat covariates were collected from nine sites within Cook County, Illinois, USA, to provide spatio-temporal information on the abundance of WNv vectors from 2002 to 2005. Regression analyses of the sampled covariates revealed that the adult *Culex* population was positively associated with temperature throughout the sampling frame. The model output also indicated that precipitation was negatively associated to mosquito abundance in 2002, 2003 and 2005 ($P < 0.05$), but positively associated in 2004 ($P < 0.05$). A land use land cover classification, based on QuickBird visible and near infra-red data, acquired at 0.61 m resolution, was used to investigate possible associations between geographical features and the abundance of sampled *Culex* oviposition surveillance sites. A maximum likelihood unsupervised classification in ArcInfo 9.2® revealed that the highest overall mosquito abundance was found in sites having a low-to-moderate range of built environment (40%) and high forest composition. A set of propagation equations were then designed to model the calibration uncertainties, which revealed that normalized difference vegetation index (NDVI), and two NDVI variants, were informative markers for the sampled mosquito data. Spatial dependence of the covariates of *Cx. restuans* and *Cx. pipiens* oviposition sites were indexed using semivariograms, which suggested that all main effects of the explanatory variables were statistically significant in the model. Additionally, a multispectral classification and digital elevation model-based geographical information system method were able to evaluate stream flow direction and accumulation for identification of terrain covariates associated with the sampled habitat data. These results demonstrate that remotely sensed operational indices can be used to identify parameters associated with field-sampled *Cx. pipiens* and *Cx. restuans* aquatic habitats.

Keywords: West Nile virus, *Culex pipiens, Culex restuans*, geographical information system, QuickBird.

Introduction

A challenge in devising effective West Nile virus (WNv) surveillance programmes is the lack of sufficient empirical knowledge on the spatio-temporal dynamics of bird-feeding mosquitoes and their relationship to dispersal, egg laying, host seeking and abundance. Previous research has shown that mosquito abundance will vary significantly in different areas due to hydrologic regime, vector control activities and the proximity to habitats and blood-meal hosts (Shaman et al., 2002; Kutz et al., 2003; Meece et al., 2003). These variations create fluctuation in abundance and distribution of virus-positive mosquitoes, virus-positive dead birds and seropositive live birds, and pose a challenge for mosquito-based prevention programmes. These variations also illus-

Corresponding author:
Benjamin G. Jacob
School of Medicine, Department of Infectious Diseases
University of Alabama at Birmingham
206C Bevill Biomedical Research Bldg
845 19th street, Birmingham, AL, 35294, USA
Tel. +1 205 996 7894; Fax +1 205 934 5600
E-mail: bjacob@uab.edu

trate the need for surveillance strategies targeting arboviral transmission. Untargeted or random interventions are inefficient, as they lack adequate empirical habitat data, since spatio-temporal distribution of organisms is often left-skewed (May, 1981; Magurran, 1988).

In general, WNv transmission is maintained at low levels in vector mosquitoes and reservoir hosts with transient, sporadic outbreaks among humans. Yet, under specific favourable conditions, WNv may exhibit high infection incidence in vectors and hosts (Epstein and Defilippo, 2001; Reisen et al., 2004; Lampman et al., 2006). Mosquito infection rates of WNv change dramatically from week to week during the amplification phase (Gu et al., 2004; Lampman et al., 2006). As a result, the focus of WNv surveillance programmes should shift from detection of mosquito infection to estimation of the magnitude of transmission intensity. To accomplish this, focused effort must be placed on regions and time periods of increased abundance of agent, reservoir or vector species, as these increases will likely indicate increased risk of arboviral transmission (Andreadis et al., 2004; Hayes et al., 2005). Improving effectiveness of WNv surveillance requires the selection of effective habitat covariates, while avoiding unwarranted, inefficient indicators of risk exposure, e.g. numbers of positive pools and minimal infection rates (MIR) (Gu et al., 2003).

Recently, the use of remote sensing (RS), geographical information systems (GIS) and geostatistical algorithms, for the prediction of geographical distributions of agent, reservoir and vector species, have been advocated to augment traditional WNv mapping methods (Nicholson and Mather, 1996; Dale et al., 1998; Hay et al., 1998, 2000; Kitron, 1998; Srivastava et al., 2001; Rogers et al., 2002; Kutz et al., 2003; Petersen et al., 2003; Brownstein et al., 2004; Ruiz et al., 2004; Griffith, 2005; Gu and Novak, 2005; Lopes et al., 2005; Sithiprasasna et al., 2005; Gu et al., 2006; Jacob et al., 2009). For example, Jacob et al. (2009) generated a land use land cover (LULC) classification in an ArcInfo 9.1® database, based on Landsat-7 Enhanced Thematic Mapper (ETM)+ data acquired in July 2003 and Landsat-5 Thematic Mapper (TM) data acquired in July 1991. These data were overlaid with 15 fixed oviposition surveillance sites of *Culex restuans* and *Culex pipiens*, two ornithophillic mosquito species thought to play a large role in the WNv enzootic cycle in Urbana-Champaign, East-Central Illinois (Lampman et al., 2006). A maximum likelihood unsupervised classification and LULC detection was performed, using a cross-tabulation detection method. The resulting LULC change matrix revealed that between 1991 and 2003, there was a total of 12.1% LULC change. The egg raft rate of *Cx. restuans* and *Cx. pipiens* was significantly higher in urban then rural LULC habitats. Quantification of vector-host interactions, incorporated on LULC maps, can reveal spatio-temporal distribution of WNv mosquito vectors. However, LULC statistics have not been developed using less than 1 m spatial resolution data for determining variation in *Culex* habitats, over short distances, based on differences in land cover.

Prediction of the satellite-derived vegetation index (VI), associated with WNv mosquito aquatic habitats, can be remarkably accurate (Linthicum et al., 1987; Huete et al., 1992; Hay et al., 2000; Backenson et al., 2002; Brownstein et al., 2002; Ward et al., 2004; Kunkel and Novak, 2005; Cooke et al., 2006; Brown et al., 2008). For example, Advanced Spaceborne Thermal Emission and Reflection Radiometer (ASTER)-derived normalized difference vegetation index (NDVI) data identified 16 sites were adult mosquitoes were captured within a densely populated urban environment in New Haven, Connecticut. Canonical correlation analysis showed a significant relationship between the variables sampled (NDVI, disease/water stress index and distance to water) and four local WNv competent vectors (*Cx. pipiens, Cx. restuans, Culex salinarius* and *Aedes vexans*) (0.93, $P \leq 0.03$), explaining 86% of the variance in the field sampled measures (Brown

et al., 2008). SPOT-5 images (10 m resolution) allowed for detailed assessment of spatio-temporal evolution of ponds, through two VI indices: i.e. the normalized difference pond index (NDPI) and the normalized difference turbidity index (NDTI), for investigating behavior of *Culex poicilipes* mosquitoes in Senegal. Using NDVI for quantitative assessments of WNv infection foci, however, raises issues related to the spatial scale associated with the remote measurements. Satellite sensors always measure radiation quantities for areas substantially larger than those sampled by field instruments (Hay et al., 2000). For example, the NDVI algorithm for identification of environmental predictors associated with WNv, in all previous research, was derived from satellite imagery, with a spatial resolution greater than 1 m. A set of uncertainty propagation equations, designed to model calibration uncertainties using sub-meter resolution data, may account for geophysical variation in *Culex* aquatic habitats, with a higher degree of accuracy and precision than moderate and coarse resolution data. Furthermore, progress has been made in the development of VIs by reducing the inherent canopy background-induced noise, atmosphere contamination and saturation problems in the NDVI. These indices include the soil-adjusted vegetation index (SAVI) and the atmospherically resistant vegetation index (ARVI). Presently, there is no published work using SAVI and ARVI for identification of WNv transmission dynamics and control measures.

Geostatistics and RS/GIS can also map variation in WNv vectors and bird populations based on differentials in environmental parameters, which can identify and validate model that link ecological factors to sampled habitat variables (Kulldroff, 1997; Andreadis et al., 2001; Eidson et al., 2001; Theophilides et al., 2006). For example, case data with spatial information from WNv epidemics, occurring in 2002 (1,377 horses), 2003 (396 horses), and 2004 (134 horses) in Texas, were analyzed by using spatial scan statistic (Poisson model) and kriging of empirical Bayes analyses. Smoothed county attack rates identified geographic locations of horses with WNv disease and spatial clusters of affected horses (hyperendemic foci), in each of the three study years (Wittich et al., 2008). Even though geostatistical models have been used in WNv research, kriged residuals have not been used to predict *Cx. restuans* and *Cx. pipiens* in a mosquito abatement district.

Satellite-derived characteristics of drainage networks and drainage basin physiographic parameters have been used in hydrologic modeling of flood and swamp water mosquito abundance (Shaman et al., 2002). Automated generation of drainage networks has become increasingly popular with the use of GIS and the availability of digital elevation models (DEM). A raster-based DEM is a continuous elevation matrix that is interpolated from contour lines, spot heights or derived through photogrammetry (Gao and Lo, 1995; Giles and Franklin, 1996). The latter produces high resolution DEM through an automatic measurement, using stereo-image matching, which can yield several catchment hydrological variables, including percent saturation and total surface runoff for identification of covariates associated with aquatic habitats of protozoan and arboviral vector mosquitoes (Patz et al., 1998; Shaman et al., 2002; Mushinzimana et al., 2006; Calhoun et al., 2007; Jacob et al., 2009). For example, Patz et al. (1998) used a water balance GIS model to hindcast weekly soil moisture levels in the Lake Victoria basin. These soil moisture levels were then associated with local human biting rates and entomologic inoculation rates. Additionally, a DEM flow distance-to-stream grid can evaluate flow direction and surface runoff for locating WNv mosquito aquatic habitat larval abundance and distribution. For example, Jacob et al. (2009) used multispectral QuickBird imagery classification and DEM-based GIS methods to evaluate stream flow direction and accumulation for identification of arboviral vector *Culex quinquefasciatus* larval abundance in urban regions of Gulu, Uganda. Euclidian distance-to-nearest hydrological body was calculated as the distance from a grid cell to a stream grid cell, as defined by a stream raster grid. The terrain analysis

using DEM (TauDEM), in ArcGIS 9.1®, was used to retrieve these parameters. A three-dimensional (3-D) model of the study area was constructed based on the DEM, using ArcScene extension of ArcGIS®. The range of the elevation in the DEM had a minimum value of 996 m, with a maximum value of 1,132 m. Results indicated that there were a significant positive correlation for *Culex* aquatic habitat larval count and slope (0.24) for the local model, based on distance to stream.

Targeted surveillance can have significant implication for WNv management in communities where allocation of limited resources should be optimized (Lampman and Novak, 1996; Gu and Novak, 2005; Gu et al., 2006). By modeling biological and spatial heterogeneity of *Cx. pipiens* and *Cx. restuans* aquatic habitats, based on mosquito productivity and ovipositional foraging, cost-effectiveness of environmental management of WNv may be achieved in a mosquito abatement district. In this research, field-sampled data and remotely-sensed wavelength ranges from the visible and near infrared (NIR) region of the QuickBird satellite, were used to determine ecological predictors associated with aquatic habitats from *Cx. pipiens* and *Cx. restuans*, a major WNv vector in Desplaines Valley mosquito abatement district (DPMAD) in Cook County, Illinois.

The objectives of this research were (i) to compute LULC indices; (ii) to establish the sensitivities and dynamic ranges of NDVI and two NDVI variants, i.e. SAVI and ARVI; (iii) to apply kriging techniques to develop spatial linear prediction models of potential larval habitat sites; and (iv) to construct a DEM to summarize *Cx. restuans* and *Cx. pipiens* aquatic habitats in DVMAD in Cook County, Illinois.

Materials and Methods

Study site

The DVMAD is located on the west side of Cook County, Illinois, USA. The DVMAD is bound to the north and east by the Chicago Department of Public Health (CDPH), to the south by the South Cook county mosquito abatement district (SCCMAD) and to the west by the Cook/Du Page county line. The district encompasses an area of 77 square miles that includes thirty-one villages (Fig. 1). The annual precipitation for the area averages 928 mm, from which August receives the highest amount of rain. The month of July records the highest temperatures throughout the year. Surveillance sites were allocated in nine villages: Brookfield, Berkeley, La Grange Highlands, River Forest, Hillside, Justice, Willow Springs, Summit and Oak Park.

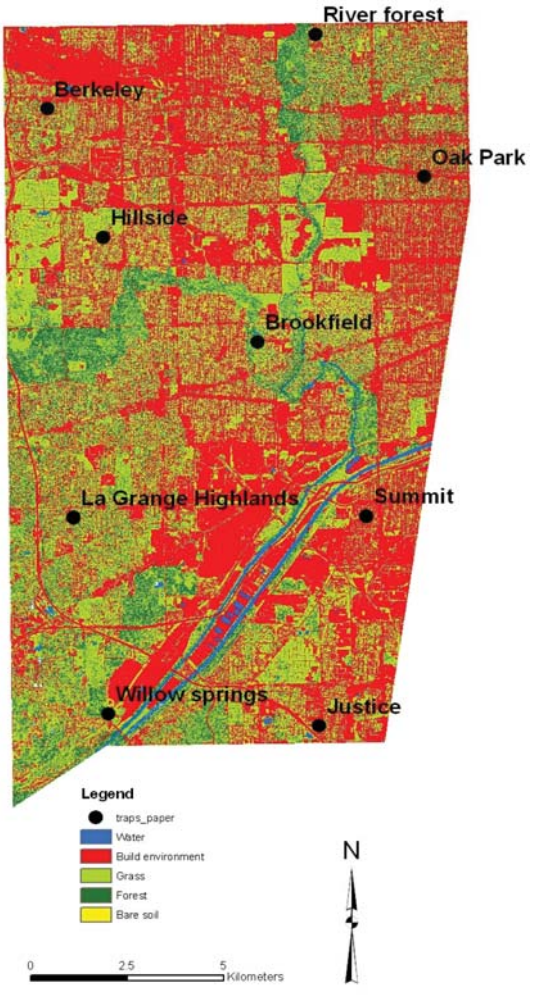

Fig. 1. Map of the Desplaines Valley mosquito abatement district (DVMAD), Cook county, Illinois, USA.

Adult mosquito sampling

Adult population levels were monitored through the use of nine gravid traps placed in each of the sites from July 2002 to July 2005. These traps were dispersed throughout the townships under charter of the abatement district. For our purpose, data were available from the gravid traps over the same time scale at the nine sites. All the specimens were identified to species using regional and national taxonomic keys (Darsie and Ward, 1981) at the main office of the DVMAD. Once data were collected, all variables (abundance, polymerase chain reaction (PCR)-positive pools and PCR-tested pools) were entered onto worksheets with the respective date of collection used to divide all data into epidemiological weeks. Ordinarily, in order to carry out epidemiological surveillance activities, disease outbreaks are grouped around a seven-day period known as the epidemiological week (Pan American Health Organization, 2000).

Satellite data classification

A QuickBird image (www.digitalglobe.com) encompassing the visible and NIR bands was acquired on July 15, 2005. QuickBird multispectral products provided four discrete non-overlapping spectral bands covering a range from 0.45 to 0.72 µm, with an 11-bit collected information depth. The QuickBird data were classified using the Iterative Self-Organizing Data Analysis Technique (ISODATA) unsupervised routine in ERDAS *Imagine* 9.1® (Atlanta, GA, USA). QuickBird Standard Imagery products are radiometrically corrected, sensor corrected, geometrically corrected and mapped to a cartographic projection (www.digitalglobe.com).

DVMAD geodatabase

Raw data from 25 rainfall and eight temperature stations, around and within the study area, was acquired from the Illinois State Water Survey. These data were also classified into epidemiological weeks. A logical design model was created and exported to a Microsoft repository using Unified Model Language (UML) in VISIO enterprise (Microsoft®). This logical ArcGIS design contained feature datasets, feature classes and tables and associations between tables and feature classes. CASE tools wizard from ArcCatalog were used to create and populate the WNv geodatabase with spatial and alphanumerical data. Spatial data included three feature classes. Alphanumerical data, on the other hand, was stored in tables, including mosquito abundance data and PCR-positive test data for a 4-year period from 2002 (Fig. 2) to 2005. Alphanumerical data were standardized by epidemiological weeks for each analyzed year.

Land use land cover classification (LULC)

All field and remote data was transferred to an ArcGIS 9.2® database (ESRI, Redlands, CA, USA) to generate five LULC classifications: built environment, forest, water, grass and bare soil. These classes were defined as follows:

Built environment - Comprised of areas of intensive use with much of the land covered by man-made physical infrastructures. This land cover class included commercial, residential, industrial, transportation and communications/utilities.

Forest - Vegetation (mainly natural) and woodland (trees >5 m tall; canopy cover 25-75%). This land cover class included mixed woodlands, grasslands and old-fields with mixed scattered trees.

Water - Permanent bodies of water such as lakes, streams, rivers, storm water retention ponds and hydrophilic vegetation. Wetlands with a high water table and areas which are often interspersed with channels or pools of open water, road side ditches, storm/rain and open channel sewers were also included in this class.

Grass - Class dominated by cultivated grasses planted in developed settings for recreation, erosion control, or aesthetic purposes. This class included parks, lawns, golf courses, airport grasses and industrial site grasses.

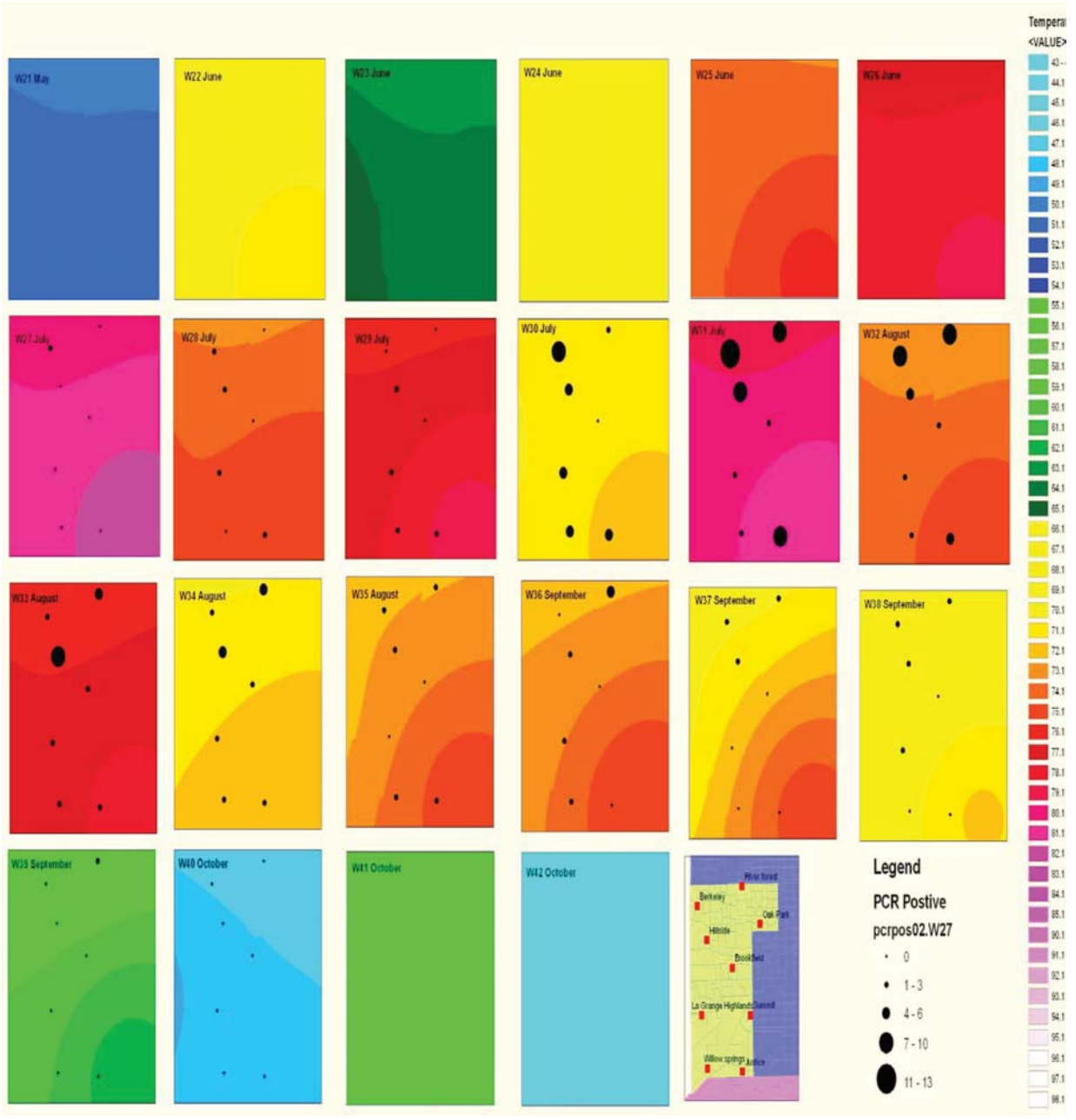

Fig. 2. Weekly PCR-positive tests for WNv and temperature for Desplaines Valley mosquito abatement district (DVMAD), Cook County, Illinois, USA (2002).

Bare Soil - Bare soil rock, sand, silt, gravel or other earthen material with little or no vegetation within urban areas. Examples of this LULC included exposed soil in urban areas and construction sites.

Python 2.5.4®, a scripting language, was used to execute methods and properties for data management using spatial analyst tools of ArcGIS 9.2®. Scripts were created to automate tasks, such as

interpolation methods using an LULC classification. Then, these temporary files were used as input for the geoprocessor, and the files were accessed using looping techniques in Python. Through this process, continuous surface grid maps were created containing interpolated values of all land cover in the study site. Then, the gravid trap feature class was overlaid on each of the continuous surface maps to assign LULC classifications to each mosquito trap.

Once the LULC map of the DVMAD was obtained, an evaluation of LULC composition was performed using 100 m and 290 m buffers for the nine trapping coordinates. LULC detection was performed using a cross-tabulation detection method.

Vegetation indices (VI)

The different modules in the Spatial Analyst extension of ArcView 9.2® and spatial modeler tools from ERDAS *Imagine* 9.1® were used to perform the VI calculations. NDVI was calculated using radiance, surface reflectance (*p*), or apparent reflectance (measured at the top of the atmosphere) values in the QuickBird red (0.63 to 0.69 µm) and NIR (0.76 to 0.90 µm) spectral bands. The ratio of reflected radiance from the red and NIR bands was used to normalize illumination and topographic variation and to form the NDVI (Tucker, 1979; Huete et al., 1994; Hay et al., 2000; Asner et al., 2003a, b). The difference of the QuickBird bands was divided by their sum, which formed the functionally equivalent NDVI. This NDVI, over terrestrial surfaces of the study site, was constrained between 0 and 1 (Jackson and Huete, 1991). The difference in reflectance was divided by the sum of the two reflectances. Raster modeling in ArcView® included: performing image differencing on NDVI layers, classifying the layers into different classes and calculating a wetness index using the Raster Calculator. NDVI was computed directly without any bias or assumptions regarding plant physiognomy, land cover class, soil type or climatic conditions, with a range from -1.0 to 1.0 from QuickBird reflectances, (*p*), using the expression:

1)

$$NDVI = \frac{\rho_{NIR} - \rho_{red}}{\rho_{NIR}\,\rho_{red}}$$

$$u^2_{cal}(NDVI) = \left(\frac{\partial NDVI}{\partial \rho_{NIR}}\right)^2 u^2_{cal}(\partial \rho_{NIR}) + \left(\frac{\partial NDVI}{\partial \rho_{red}}\right)$$

$$u^2_{cal}(\partial \rho_{red}) + 2\ \frac{\partial NDVI}{\partial \rho_{NIR}}\ \ \frac{\partial NDVI}{\partial \rho_{red}}\ \bullet\ u_{cal}(\rho_{NIR}, \rho_{red})$$

$$\frac{\partial NDVI}{\partial \rho_{NIR}} = \frac{2\rho_{red}}{(\rho_{NIR} + \rho_{red})^2}$$

$$\frac{\partial NDVI}{\partial \rho_{red}} = \frac{-2\rho_{NIR}}{(\rho_{NIR} + \rho_{red})^2}$$

$$\frac{\partial NDVI}{\partial \rho_{NIR}}\ \ \frac{\partial NDVI}{\partial \rho_{red}} = \frac{-4\rho_{NIR}\,\rho_{red}}{(\rho_{NIR} + \rho_{red})^2}$$

To account for changing soil brightness, SAVI was also calculated, utilizing an adjustment factor L that effectively shifted the origin of vegetation isolines in NIR/VIS reflectance space. The SAVI utilizes a constant *L* to remove the soil background noise (Huete, 1988). For high vegetation cover, the value of *L* is 0.0, and *L* is 1.0 for low vegetation cover. For intermediate vegetation cover, L = 0.5 is the value which is most widely used in generating SAVI (Huete, 1988). The appearance of *L* in the multiplier causes of SAVI have a range identical to the NDVI (-1.0 to 1.0) (Huete et al., 1992). The net result is an NDVI with an origin not at the point of zero, red and NIR reflectances. In this research, SAVI was calculated using radiance, surface reflectance, *p*, in the QuickBird red and NIR spectral bands. SAVI was calculated where *L* was a plant height adjustment factor that accounted for differential red and NIR extinction through the year. In this research, *L* = 0.5 was used for all *Cx. pipiens* and *Cx. restuans* aquatic habitats sampled in the study site. The SAVI was calculated as:

2)

$$SAVI = (1+L)\frac{\rho_{NIR} - \rho_{red}}{\rho_{NIR} + \rho_{red} + L}$$

$$u^2_{cal}(SAVI) = \left(\frac{\partial SAVI}{\partial \rho_{NIR}}\right)^2 u^2_{cal}(\rho_{red}) + \left(\frac{\partial SAVI}{\partial \rho_{red}}\right)^2$$

$$u^2_{cal}(\rho_{red}) + 2\ \frac{\partial SAVI}{\partial \rho_{NIR}}\ \ \frac{\partial SAVI}{\partial \rho_{red}}\ \bullet\ u_{cal}(\rho_{NIR}\rho_{red})$$

where

$$\frac{\partial SAVI}{\partial \rho_{NIR}} = (1+L)\ \frac{2\rho_{red}+L}{(\rho_{NIR} + \rho_{red}+L)^2}$$

$$\frac{\partial SAVI}{\partial \rho_{red}} = (1+L)\ \frac{-2\rho_{NIR}+L}{(\rho_{NIR} + \rho_{red}+L)^2}$$

It was of interest to determine how the blue band inclusion into the VI would identify land cover for making inferences of *Cx. pipiens* and *Cx. restuans* aquatic habitat features. The resistance of the ARVI to atmospheric effects, in comparison to NDVI, was accomplished by a self-correction process for the atmospheric effect on the QuickBird red channel, using the difference between the blue and red channels to correct the radiance in the red channel. Aerosols absorbing gases, such as water vapor, and undetected clouds, affect upwelling radiances measured by satellite instruments (Kaufman and Tanre, 1992; Hay et al., 1998). An ARVI was developed, from the vegetation land cover attributes, using the QuickBird data. ARVI was calculated using radiance, surface reflectance (*p)* in the QuickBird blue channel (0.05 to 0.06 µm), red and NIR spectral bands. A single value of γ = 1.0 was used to substantially reduce the sensitivity of atmospheric effects. The ARVI was defined as:

$$ARVI = \frac{\rho_{NIR} - \rho_{rb}}{\rho_{NIR} + \rho_{rb}}$$

where

$$\rho_{rb} = \rho_{red} - \gamma(\rho_{blue}\ \ \rho_{red})$$

and

$$u^2_{cal}(ARVI) = \left(\frac{\partial ARVI}{\partial \rho_{NIR}}\right)^2 u^2_{cal}(\rho_{NIR}) + \left(\frac{\partial ARVI}{\partial \rho_{red}}\right)^2 \bullet$$

$$u^2_{cal}(\rho_{blue}) + \left(\frac{\partial ARVI}{\partial \rho_{blue}}\right)^2 \bullet u^2_{cal}(\rho_{blue}) + \frac{\partial SAVI}{\partial \rho_{NIR}}\ \ \frac{\partial SAVI}{\partial \rho_{blue}}$$

where

$$\frac{\partial ARVI}{\partial \rho_{NIR}} = \frac{2\rho_{rb}}{(\rho_{NIR} + \rho_{rb})^2}$$

$$\frac{\partial ARVI}{\partial \rho_{red}} = \frac{-2(1+\gamma)\rho_{NIR}}{(\rho_{NIR} + \rho_{rb})^2}$$

$$\frac{\partial ARVI}{\partial \rho_{blue}} = \frac{2\gamma\rho_{NIR}}{(\rho_{NIR} + \rho_{rb})^2}$$

The different modules within the ArcView® Spatial Analyst and spatial modeler tools from ERDAS Imagine 9.1® were used to perform the VI calculations. The imagine format files, however, were not always accessible in all modules of the ArcView® software and its extensions. Thus, the decision was made to convert the imagine format files to Arc/Info® GRID files and recalculate all VI equations in ArcView Spatial Analyst. This procedure produced an Arc/Info® GRID format file with a floating-point data range of -1 to 1. Randomly selected *Cx. restuans* and *Cx. pipiens* aquatic habitat locations, from all file formats, were compared to ensure correct calculation of all VIs in Spatial Analyst. The VI calculations resulted in a grid file which stored all calculated floating-point values. The validation was performed by identifying and recording X, Y coordinates from the Imagine format data images, recording the VI values at specific locations, and then pointing to the corresponding locations in the Arc/Info GRID format file and compar-

ing values. This process was useful for calculation and validation of all models, as well as for verifying floating-point values.

Values for NDVI were successfully aggregated and overlaid onto georeferenced field-based data for the study site. The VIs were used to select all *Cx. restuans* and *Cx. pipiens* aquatic habitats with heavy, moderate and low vegetated values. A database was generated with the mean, minimum, maximum and standard deviations for VI data aggregated to the habitat level. VIs have the benefit that pixels are not forced into inappropriate land cover classes, but instead provide a proportional measure of vegetation (Bannari et al., 1995). The VI datasets were then merged with the entomological datasets.

Leaf area index (LAI)

Sensitivity analysis was conducted on the NDVI and the NDVI variants by analyzing the atmospheric and soil-perturbed responses, as a continuous function of plant leaf area index (LAI). Randomly selected grid cell and spectral measurements were assessed to determine plant LAI in ArcMap. The LAI was used to predict the photosynthetical primary production, as it is was related to the sampled *Cx. restuans* and *Cx. pipiens* data collected in the study site. In past research, remotely sensed data has been combined with meteorological data to estimate the NDTI, which can provide a measure of the moisture availability using the ratio of actual to potential evapotranspiration related to vector mosquitoes (Lacaux et al., 2006). In this research, an inverse exponential relation between LAI and light interception, which was linearly proportional to the primary production rate, was established using:

$$P = P_{\max}\,(1\text{-}e^{-c \cdot LAI})$$

where $P_{\max}$ signifies the maximum primary production and c signifies a plant growth coefficient. This inverse exponential function was used as the primary production function, including levels of evapotranspiration (Pierce and Running, 1988). The LAI was determined directly by taking a statistically significant sample of plants from a crop, measuring the mean leaf area per plant and dividing it by the mean available land surface per plant. The indirect method measures light extinction and relates it to LAI (Hay et al., 2000). The atmospherically resistant version minimized atmospheric noise, but enhanced soil noise. Likewise, the soil-adjusted variant minimized soil noise, but remained sensitive to the atmosphere. The SAVI and ARVI had a relative error of 20% and VEN of +/- 0.28 LAI and +/- 0.26. The NDVI had a relative error of 25% and VEN of +/- 0.82 LAI.

Spatial analyses

Spatial linear prediction was performed initially using kriging. In this research, kriging residuals were generated using a two step process: the fitting of a semivariogram model function (of distance), followed by the solution of a set of matrix equations (Deutsch and Journel, 1992). Geostatistical techniques were used to interpolate the value $Z(x_0)$ [*Cx. restuans* and *Cx. pipiens* habitat of the DVMAD study site $Z(x)$] at an unobserved *Culex* habitat location x_0 from field and remote sampled covariates $z_i = Z(x_i)$, I = 1,…, n of the study site, at nearby habitat locations $x_1 \ldots x_n$. Kriging computes the best linear unbiased estimator of $Z(x_0)$, based on a stochastic model of the spatial dependence quantified either by the variogram $\gamma(x,y)$, or by expectation $\mu(x) = E[Z(x)]$ and the covariance function $c(x,y)$ of the random field (Krige, 1966). The kriging estimator was given by a linear combination:

$$\hat{Z}(x_0) = \sum_{i=1}^{n} \omega_i(x_0) Z(x_i)$$

of the *Cx. restuans* and *Cx. pipiens* aquatic habitat covariates $z_i = Z(x_i)$ with their weights chosen such that the variance:

$$\sigma_k^2(x_0) = \mathrm{Var}\left(\hat{Z}(x_0) - Z(x)\right) = \sum_{i=1}^{n} \sum_{j=1}^{n} \omega_i(x_0)\omega_j(x_0)$$

$$c(x_i, x_j) Z(x_i) + \mathrm{Var}\left(Z(x)\right) - 2 \sum_{i=1}^{n} \omega_i(x_0) c(x_i, x_0)$$

was minimized subject to the unbiasedness condition:

$$E[\hat{Z}(x)\text{-}Z(x)] = \sum_{i=1}^{n} \omega_i(x_0)\mu(x_0) = 0$$

In this research, the dependent variable was the adult count of *Cx. restuans* and *Cx. pipiens* aquatic habitats was transformed to fulfill the diagnostic normality test prior to performing kriging. The sampling site was the *Culex* aquatic habitat in the study site, but the adult *Cx. pipiens* and *Cx. restuans* counts were used as an indicator of the local density based on the gridded area.

The kriging weights of ordinary kriging were used to fulfill the unbiasedness condition of the ecologically sampled *Cx. pipiens* and *Cx. restuans* data using:

$$\sum_{i=1}^{n} \lambda_i = 1$$

and was given by the ordinary kriging equation system:

$$\begin{pmatrix} \lambda_1 \\ \\ \lambda_n \\ \mu \end{pmatrix} = \begin{pmatrix} \gamma(x_1, x_1) & \cdots & \gamma(x_1, x_n) & 1 \\ \vdots & \ddots & \vdots & \vdots \\ \gamma(x_n, x_1) & \cdots & \gamma(x_n, x_n) & 1 \\ 1 & \cdots & 1 & 0 \end{pmatrix}^{-1} \begin{pmatrix} \gamma(x_1, x^*) \\ \vdots \\ \gamma(x_n, x^*) \\ 1 \end{pmatrix}$$

The additional parameter was a Lagrange multiplier used in the minimization of the kriging error $\sigma_k^2(x_0)$ to honor the unbiasedness condition. The interpolation by ordinary kriging was given by:

$$\hat{Z}(x_0) = \begin{pmatrix} \lambda_1 \\ \vdots \\ \lambda_n \end{pmatrix}' \begin{pmatrix} Z(x_1) \\ \vdots \\ Z(x_n) \end{pmatrix}$$

The ordinary kriging error model was given by:

$$\mathrm{Var}\left(\hat{Z}(x_0)\text{-}Z(x_0)\right) = \underbrace{c(x_0, x_0)}_{\mathrm{Var}\left(Z(x_0)\right)} - \underbrace{\begin{pmatrix} c(x_1, x_0) \\ \vdots \\ c(x_n, x_0) \end{pmatrix}' \begin{pmatrix} c(x_1, x_1) & \cdots & c(x_1, x_n) \\ \vdots & \ddots & \vdots \\ c(x_n, x_1) & \cdots & c(x_n, x_n) \end{pmatrix}^{-1} \begin{pmatrix} c(x_1, x_0) \\ \vdots \\ c(x_n, x_0) \end{pmatrix}}_{\mathrm{Var}\left(\hat{Z}(x)\right)}$$

A semivariogram was used to measure spatial interaction in both the field and remotely sampled *Cx. pipiens* and *Cx. restuans* aquatic habitat data. Prediction by kriging for mosquito habitat data analyses can be based on the assumption that covariance between habitats is entirely a function of distance between habitats, as modeled by means of the semiovariogram (Kleinschmidt et al., 2001). Semivariograms were generated in ArcGIS Spatial Analyst to obtain a spatial model for kriging and to examine spatial patterns in the *Cx. pipiens* and *Cx. restuans* aquatic habitat data.

Digital elevation model (DEM)

A 3-D model of the study area was constructed based on the DEM using ArcScene extension of ArcGIS. The DEM used in this study was a raster representation of a continuous surface, originating from the Shuttle Radar Topography Mission (SRTM). Data from SRTM version 2 (i.e. finished version) were downloaded from http://srtm.usgs.gov/. For our spatial hydrological analyses, data were loaded from every 1-arc second, representing 80% of the Earth's surface, with 16 m accuracy. Differences in elevation were defined from radar interferometry, using the 2000 Endeavor mission data, which used two radar images from different, ecologically sampled *Cx. restuans* and *Cx. pipiens* aquatic habitat locations. Differences in habitat elevation were then calculated for the georeferenced habitats. All sampled *Cx. restuans* and *Cx. pipiens* aquatic habitat covariates were defined by geocoordinates, in a tiled format or within a digital rectangle. This allowed specific elevation for each individual *Cx. restuans* and *Cx. pipiens* aquatic habitat to be evaluated.

After zooming into the area of interest (AOI) (which ranged from a scale of 1:61,642,554 to 1:118), the "Downloads" button was highlighted. It was necessary to use the "modify data request", then click "SRTM 3 arc sec", and specify "GeoTiff" in the drop down menu. After "saving changes and returning to summary" the image was ready for downloading. It should be noted that no greater than 250 Mb of data was highlighted at one time, so we were able to identify subsections of the imagery. The SRTM data was available across the globe at a 90 m resolution.

Results

The LULC map of the DVMAD was dominated by built environment (≈48%) and grass (≈38%). Water accounted for less than 2% of the LULC, while bare soil represented less than 1%. Forest (≈12%) was concentrated towards the central and northern levy of the Desplaines River. The LULC compositions differed between the 100 m buffer and the 290 m buffer. Using the 100 m buffer, only the LULC compositions of Berkley and Oak Park, among the nine surveillance sites, were not significantly different at 0.05 (Fig. 3). Using only the 290 m buffer, only Justice and Berkley varied in composition between buffers at the 0.05 significance level.

Table 1 shows the results of the regression analysis output, where the variable *Culex* adult abundance was modeled in terms of precipitation, temperature and gravid trap location. In every year, the regression models were able to classify between

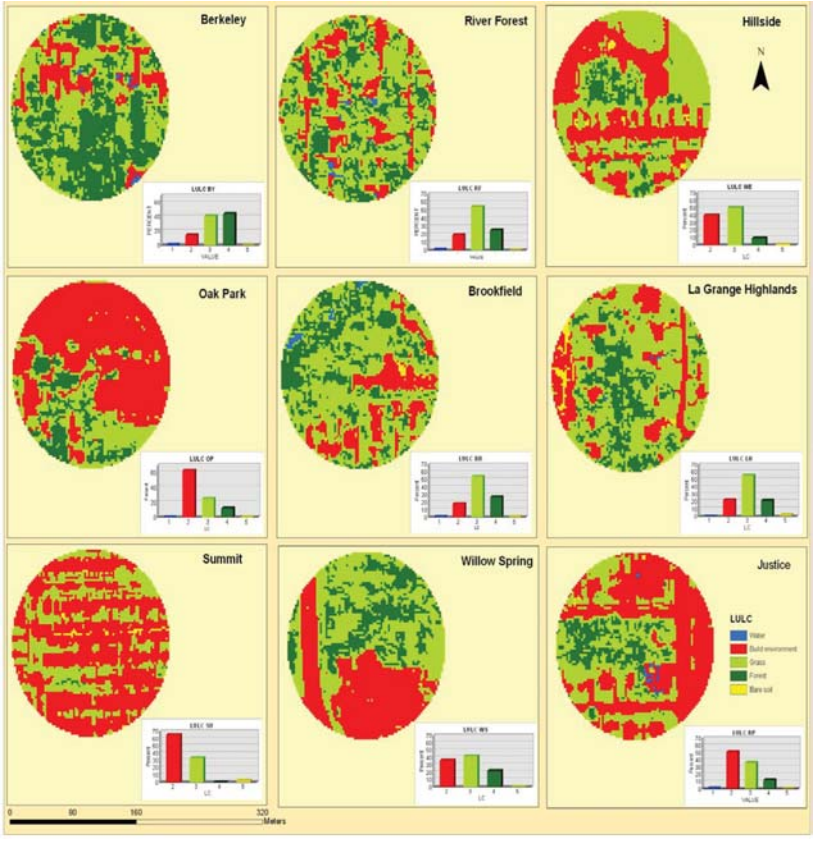

Fig. 3. Land use land cover (LULC) and 100 m buffer composition analysis for *Culex* abundance in Desplaines Valley mosquito abatement district (DVMAD), Cook County, Illinois, USA.

gravid traps with high and low abundance. Temperature and precipitation data had a significant association with *Culex* adult abundance. Throughout the study period, temperature showed a significant positive relationship with *Cx. restuans* and *Cx. pipiens* abundance (P <0.001). The variable precipitation presented a significant negative relationship (P <0.05) for the years 2002, 2003 and

Table 1. Principal determinants of mosquito adult abundance in Desplaines Valley mosquito abatement district (DVMAD).

Year	Dependent variable	Independent variable	Parameter estimate	P-value	Adj R^2	Model P
2002	Abundance°	Intercept	-8.85	<0.001	0.73	<0.001
		Temperature	0.14	<0.001		
		Rain2(log)**	-3.46	<0.001		
		Tmp*rain[a]	-3.69	<0.001		
		Berkeley	3.85	<0.001		
		River Forest	3.54	<0.001		
		Hillside	3.26	<0.001		
		Justice	2.77	<0.001		
		La Grange Highlands	2.73	<0.001		
		Willow Spring	2.64	<0.001		
		Brookfield	2.58	<0.001		
		Summit	Lowest			
2003	Abundance°	Intercept	-3.99	<0.001	0.65	<0.001
		Temperature	0.09	<0.001		
		Rain2(log)	-6.72	<0.001		
		Tmp*rain	0.09	<0.001		
		River Forest*	2.90	<0.001		
		Justice	2.30	<0.001		
		Hillside	2.26	<0.001		
		Berkeley	1.96	<0.001		
		Oak Park	1.86	<0.001		
		Brookfield	1.75	<0.001		
		La Grange High	1.70	<0.001		
		Willow Spring	1.14	<0.001		
		Summit	Lowest			
2004	Abundance°	Intercept	-7.97	<0.001	0.47	<0.001
		Temperature	0.17	<0.001		
		Rain2(Log)	4.74	0.040		
		Temp*rain	-0.06	0.050		
		Hillside	1.23	0.001		
		Oak Park	1.13	<0.001		
		Berkeley	1.03	0.001		
		Summit	0.90	0.005		
		River Forest	0.83	0.009		
		Justice	1.64	>0.15		
		Brookfield	0.35	>0.15		
		La Grange Highlands	0.27	>0.15		
		Willow Springs	Lowest	>0.15		
2005	Abundance°	Intercept	0	0.050	0.60	<0.001
		Temperature	0.09	<0.001		
		Rain2(log)	-4.84	0.050		
		River Forest	1.90	<0.001		
		Willow Spring	1.43	<0.001		
		Oak Park*	1.01	0.001		
		Berkeley*	0.92	<0.001		
		La Grange Highlands	0.40	0.050		
		Justice	0.44	0.060		
		Summit	-0.19	0.100		
		Brookfield	Lowest	>0.15		

Note: *8 Dummy variables as fixed effect were created to represent the location of each light trap in the regression model.

** Represent a two weeks lag of rainfall. It was log (rainfall+1) transformed.

[a] Represent the interaction between temperature and precipitation.

° Dependent variable was log(abundance+1) transformed.

2005. In 2004, the precipitation parameter suggested a positive relationship (P <0.05) with adult counts of *Cx. restuans* and *Cx. pipiens*.

In 2002, the overall accuracy of the model was 73.1%, while the model predicted 65.2% in 2003, 47.1% in 2004 and 60.0% in 2005. The meteorological covariates temperature, rainfall and precipitation, explained 80.1% of the variation in the model. River Forest had the highest overall *Cx. restuans* and *Cx. pipiens* adult abundance count, followed by Berkeley and Hillside, respectively. Notably, these sites had a low-to-moderate range of built environment (>40%) with high forest composition. Summit had the highest levels of built environment LULC (64.0%) and the highest *Culex* adult abundance in 2004.

Soil and atmospheric influences in the NDVI, as well as in the NDVI variants, were examined. The NDVI was sensitive to the presence of vegetation. The change in the soil background did alter the red and NIR plant reflectance and calculated SAVI (Fig. 4). The ARVI minimized atmospheric noise in the study site and did not enhance soil noise. The NDVI had the highest levels of noise and error; whereas, the NDVI variant equations partially removed soil and/or atmospheric noise to varying degrees. Soil and atmospheric effects are interactive and vary with vegetation cover, as well as produce a very complex effect on VIs (Baret and Guyot, 1991). ARVI has a similar dynamic range to the NDVI, but is on the average four times less sensitive to atmospheric effects than the NDVI (Kaufman and Tanre,

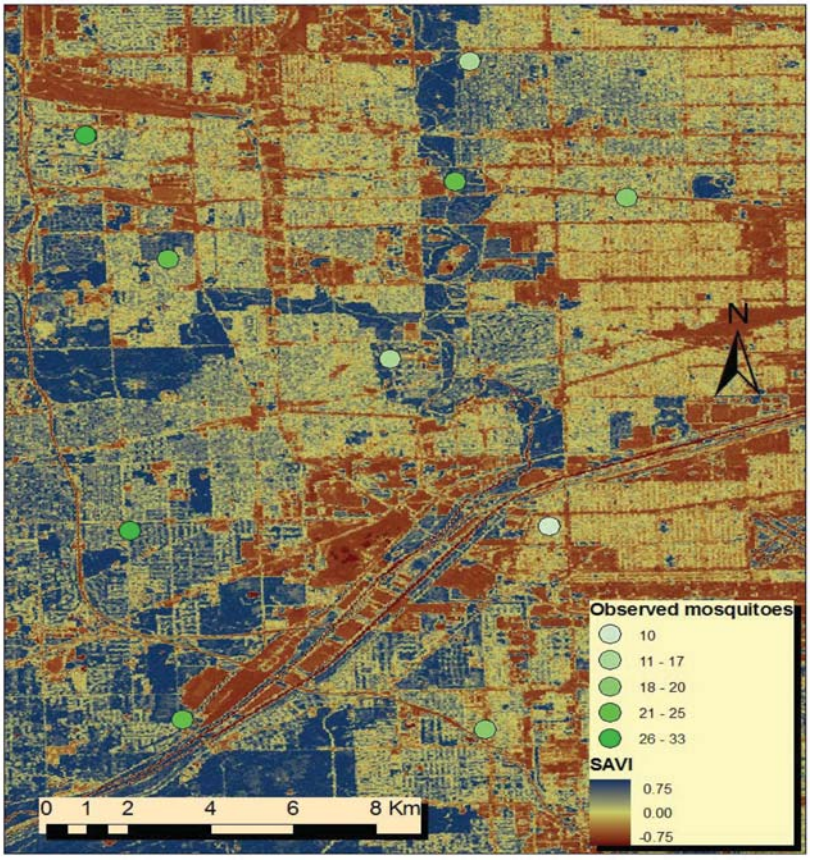

Fig. 4. Soil adjusted vegetation index (ARVI) of the *Cx. pipiens* and *Cx. restuans* aquatic habitats in Desplaines Valley mosquito abatement district (DVMAD).

1992). In these analyses, VI equations were associated with *Cx. restuans* and *Cx. pipiens* aquatic habitat abundance and distribution.

A Stream Raster Grid was generated in ArcGIS. Euclidian distance to nearest hydrological body was calculated as the distance from a grid cell to a stream grid cell, defined by a Stream Raster Grid (Fig. 5). The results showed that flow distance to stream can affect availability of *Cx. restuans* and *Cx. pipiens* aquatic habitats and calculated the distance from a grid cell moving downstream to a stream grid cell, which was defined by the Stream Raster Grid. The range of the elevation in the DEM had a minimum value of 0 m, with a maximum value of 425 m.

A first order trend ordinary kriging process was used to analyze the sampled covariates of *Cx. pipiens* and *Cx. restuans* in the DVMAD study site. An anistrophic spherical model was fitted to the semivariogram, for the ordinary kriged model using a range of 0.166, a nugget of 0, a lag size of 0.014 with 12 lags, and a partial sill of 17.95 for the study site (Fig. 6).

Discussion

As WNv and its associated vectors continue to threaten local regions, identifying tools to understand and predict risk factors can result in more efficient prevention methods. The results of this research suggest that community level spatial modeling can aid in the understanding of the biological construct of WNv. In addition, spatial modeling can facilitate early detection and resource targeting.

Data obtained in this study suggest a significant positive association between temperature and *Culex* adult abundance and a negative association between precipitation and *Culex* abundance. These findings support previous findings in which arboviral mosquito abundances were associated with temperature. For example, studies have found that St. Louis encephalitis (SLE) cases are associated with warmer temperatures and low water table levels (Shaman et al., 2002). Higher temperatures enhance microbial growth on which mosquito larvae feed (Ramachandra, 1984) and overwintering mosquito populations may be the cause of WNv outbreaks during drier seasons (Landesman et al., 2007). *Cx. pipiens* is believed to be more commonly infected with WNv and more capable of transmission during warmer temperatures (Dohm et al., 2002). The negative association between precipitation and *Culex* abundance in three of the years, and the positive relationship in one year may be due to flooding of container habitats and subsequent ground pooling.

The raster files generated from ArcView® of NDVI, SAVI and ARVI were able to identify land cover for making inferences of *Cx. restuans* and *Cx. pipiens* habitat abundance and distribution. The results documented a significant association between the VIs generated and *Cx. restuans* and *Cx. pipiens* adult abundance. Ruiz et al. (2004) used several factors related to the physical environment, such as elevation range, physiographic region, and percentage of vegetation cover, to determine WNv risk during the 2002 outbreak in the Chicago area. Diuk-Wasser et al. (2006) developed regression models to predict high and low adult mosquito abundance sites for determining arboviral activity in Fairfield county, Connecticut. The best predictive models included non-forested areas for *Cx. pipiens*, surface water and distance to estuaries for *Cx. salinarius,* surface water and grasslands/agriculture and seasonal difference in the NDVI. In agreement with these findings, our results documented a significant association between VIs, and *Cx. restuan* and *Cx. pipiens* distribution and abundance.

Mapping meterological parameters and LULC data, in Python® using spatial analytical tools from ArcGIS® database, identified land cover supporting large numbers of WNv vector mosquitoes. For example, although a highly "built environment" classified area alone was not associated with high numbers of *Culex* mosquitoes, heavy precipitation in "built environment" was found to have the largest adult mosquito abundances. Summit was found to be a poor site for *Culex* adult abundance and WNv positives overall, but, in 2004 with heavy

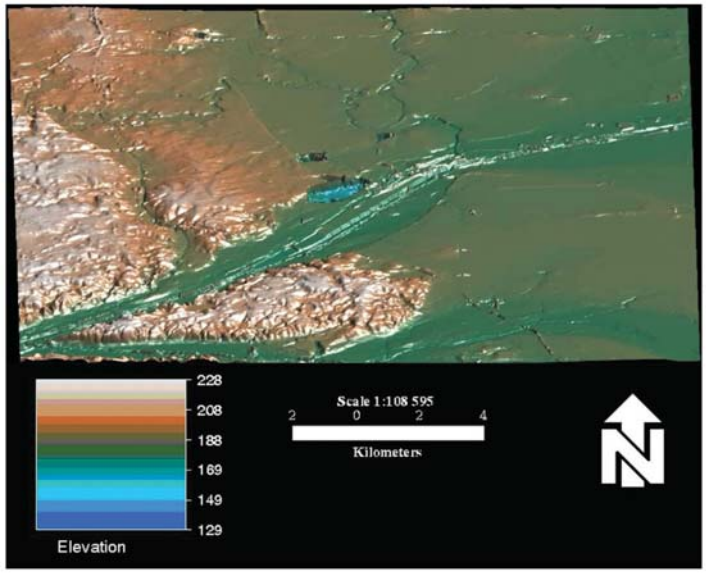

Fig. 5. Spatial hydrological model of the *Cx. pipiens* and *Cx. restuans* aquatic habitats in Desplaines Valley mosquito abatement district (DVMAD).

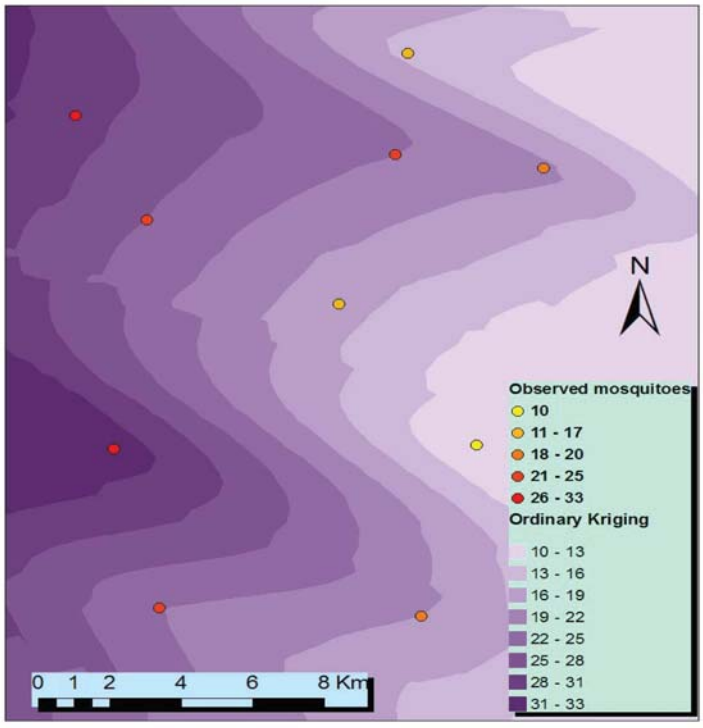

Fig. 6. Ordinary kriged residuals of adult abundance of *Cx. pipiens* and *Cx. restuans* for the Desplaines Valley mosquito abatement district (DVMAD).

rainfall, high adult counts of *Cx. pipiens* and *Cx. restuans* were found. Spatial configuration of land cover, combined with heavy rainfall, can generate numerous, temporary *Culex* aquatic habitats. Meteorological variables are considered important drivers of mosquito population abundance and spatial distribution (Kunkel and Novak, 2005). Rainfall provides surface water in which gravid females can lay eggs (Charlwood et al., 1995), which increases relative humidity, modifies temperature, and affects location and abundance of mosquito aquatic habitats (Pampana, 1969). The combined effect of rainfall and urban land cover may have aggravated the problem of WNv by supporting prodigious number of *Culex* mosquitoes with high vectorial capacity.

Site-specific land cover features may be associated with *Cx. pipiens* and *Cx. restuans* habitat abundance and distribution. For example, the Brookfield site increased in mosquito and viral detection during 2004. This site had the second largest composition of forest (27%) and grass (51%). The presence of infected, abundant WNv vector mosquitoes near trees suggests aggregation around bird habitats. It is possible that flow paths of extracted rivers are influenced by forests with a dense tree canopy, which, in turn, may influence *Culex* aquatic habitat abundance and mosquito feeding sites. Frequent blood feeding can occur by *Culex* mosquitoes on abundant passerine birds, such as the Common Grackle, and the Northern Mockingbird which occupy canopy habitats (Beveroth et al., 2005). Data collected using the 100 m buffer for Berkley confirmed that a highly productive site was associated with forest landscape (43% of composition). Gu et al. (2006) identified areas with higher WNv potential transmission intensities adjacent to the Des Plaines River, where there existed a landmark corridor harbouring disproportionately large areas of natural woodlands.

The DEM found that *Cx. restuans* and *Cx. pipiens* adult abundance were positively associated with the covariate distance from the stream. Aquatic habitats further away from the stream are likely to be rich in organic matter than those closer to the stream, as they are least likely to be diluted by surface run-off from the stream (Jacob et al., 2009). Gravid traps prevalent in valley bottoms had more *Cx. restuans* and *Cx. pipiens* than those on hills. Previous research supports the biological plausibility of this phenomenon by showing that *Culex* species does not thrive at high elevations due to cooler temperatures and lower potential for standing water habitats in valleys (Ahumada et al., 2004; Joy and Sullivan, 2005).

The semivariogram described the spatial dependence, between the field and remotely sampled measurements of *Cx. pipiens* and *Cx. restuan* aquatic habitats, as a function of the distance between the aquatic habitats. The model allowed for the estimation of the adult *Culex* count data of a sampled aquatic habitat at any point in the study site. The interpolation accuracy of the kriged-based algorithm revealed that all model coefficients and remote sampling characteristics including: surface type, sampling pattern, noise level, and strength of small-scale spatial correlation between the *Cx. restuans* and *Cx pipiens* oviposition surveillance sites, were estimated in the residuals. In this research, the estimation of the residuals was an iterative process: first, the models were estimated using the ordinary least squares estimation; then, the covariance function of the residuals were used to obtain the general least square coefficients. Interpolation accuracy was measured by the natural logarithm of the mean squared interpolation error, which revealed that all main effects of the covariates and several covariate interactions were statistically significant. The results suggest that data smoothing and stochastic techniques can estimate the risk of WNv occurrence using ecological sampled *Cx. restuans* and *Cx. restuans* aquatic habitat covariates, which can allow for quantification of error in all models generated using the site specific sampled data.

Geostatistical algorithms and remotely-sampled data in GIS can enhance the efficiency of early detection of *Cx. pipiens* and *Cx. restuan*s. Early detection is critical, because the timing of WNv actvity is important for understanding the intrica-

cies of viral amplification, as well as extending the window for intervention. In temperate areas, the initiation of arboviral transmission cycles is often associated with low vector densities and low levels of transmission (Gu et al., 2008). However, collection of sufficient mosquito samples, for obtaining sensible detetction power, can be difficult when mosquito abundance is low. Detection of mosquito infection, when there is low transmission, requires collections of large samples of mosquitoes. Seven hundred mosquitoes are needed for a modest detetction probability of 0.5, when the natural infection rate is 0.1% (Gu and Novak, 2005). As a result, non-detection is common in areas of low WNv transmission. However, identification of remotely sensed targeted sites, using geostatiscal algorithms, can reduce uncertainties in sampling strategies and can improve epidemiological intelligence of arboviruses, even when transmission foci are sporadic and mosquito infection is low. Accumulated knowledge of the environmental heterogeneity of *Cx. restuans* and *Cx. pipiens,* using simple field-based models, can assist in identifying 'hotspots' for remotely targeted surveillance. Assuming that the epidemiological intelligence about the hotspots is correct, a targeted surveillance can yield higher sensitivity and efficiency than random surveillance for a fixed surveillance investment.

In conclusion, forest and built environment LULCs at the DVMAD study site, for our selected time period, was associated with adult abundance of *Cx. restuans* and *Cx. pipiens* at nine fixed surveillance sites. NDVI, SAVI and ARVI data derived from the QuickBird visible and NIR was able to determine ecological conditions in the study site. Spatial interpolation techniques, using ordinary kriging, was able to characterize habitats based on the adult *Culex* counts for generating a predictive map. DEM statistics were able to identify terrain covariates associated with *Cx. restuans* and *Cx. pipiens* aquatic habitats. Future field and remote data collections in the DVMAD study site should include more data on wild birds as reservoir hosts, including roosting habitats, foraging ranges and migratory routes, and on horses and humans as accidental hosts.

Acknowledgements

We acknowledge the data collection provided by the DVMAD field collection teams for conducting this study. This research was funded by the National Institutes of Health Grant U01A154889 (Robert J. Novak), University of Alabama at Birmigham.

References

Ahumada JA, LaPointe D, Samuel MD, 2004. Modeling the population dynamics of *Culex quinquefasciatus* (Diptera: Culicidae), along an elevation gradient in Hawaii. J Med Entomol 41, 1157-1170.

Andreadis TG, Anderson JF, Vossbrink CR, 2001. Mosquito surveillance for West Nile virus in Connecticut, 2000: isolation from *Culex pipiens, Cx. restuans, Cx. salinarius* and *Culiseta melanura*. Emerg Infect Dis 7, 670-674.

Andreadis TG, Anderson JF, Vossbrinck CR, Main AJ, 2004. Epidemiology of West Nile virus in Connecticut: a five year analysis of mosquito data 1999-2003. Vector Borne Zoonotic Dis 4, 360-378.

Asner G, Hicke J, Lobell D, 2003a. Per-pixel analysis of forest structure: vegetation indices, spectral mixture analysis and canopy reflectance modeling. In: Wulder M, Franklin S (Eds). Remote Sensing of Forest Environments: Concepts and Case Studies. Boston: Kluwer Academic, pp. 229-254.

Asner GP, Scurlock JMO, Hicke JA, 2003b. Global synthesis of leaf area index observations: implications for ecological and remote sensing studies. Global Ecol Biogeo 12, 191-205.

Backenson PB, White DJ, Eidson M, Kramer LD, Morse DL, Tucker CJ, Myers MF, Hay SI, Rogers DJ, 2002. Mapping of West Nile virus risk in the Northeast United States using multi-temporal meteorological satellite data. In: Rigby J, Skelly C and Whigham PA (Eds). Proceedings of GeoHealth 2002: Supporting Decison Making in Health, 3-5 Dec, Wellington, New Zealand. University of Otago, ISBN 1877139580, pp. 165-166.

Bannari A, Morin D, Bernie GB, Bonn FJ, 1995. A theoretical review of different mathematical models of geometric corrections applied to remote sensing images. Remote Sens

Rev 13, 27-34.

Baret F, Guyot G, 1991. Potentials and limits of vegetation indices for LAI and APAR assessment. Remote Sens Environ 35, 161-173.

Beveroth TA, Ward MP, Lampman RL, Ringia AM, Novak RJ, 2005. Changes in seroprevalence of West Nile virus across Illinois in free-ranging birds from 2001 through 2004. Am J Trop Med Hyg 74, 174-179.

Brown HE, Diuk-Wasser MA, Guan Y, Caskey S, Fish D, 2008. Comparison of three satellite sensors at three spatial scales to predict larval mosquito presence in Connecticut wetlands. Remote Sens Environ 112, 2301-2308.

Brownstein JS, Holfold TR, Fish D, 2004. Enhancing West Nile virus surveillance, United States. Emerg Infect Dis 10, 1129-1133.

Brownstein JS, Rosen H, Purdy D, Miller JR, Merlino M, Mostashari F, Fish D, 2002. Spatial analysis of West Nile virus: a rapid risk assessment of an introduced vector borne zoonosis. Vector Borne Zoonotic Dis 2, 157-164.

Calhoun LM, Avery M, Jones L, Gunarto K, King R, Roberts J, Burkot TR, 2007. Combined sewage overflows (CSO) are major urban breeding sites for *Culex quinquesfasciatus* in Atlanta, Georgia. Am J Trop Med Hyg 77, 478-484.

Charlwood JD, Smith T, Kihonda J, Heiz B, Billingsley PF, Takken W, 1995. Density independent feeding success of malaria vectors (Diptera: Culicidae) in Tanzania. Bull Entomol Res 85, 29-35.

Cooke WH III, Grala K, Wallis RC, 2006. Avian GIS models signal human risk for West Nile virus in Mississippi. Int J Health Geograph 5, 36.

Dale PE, Ritchie SA, Territo BM, Morris CD, Muhar A, Kay BH, 1998. An overview of remote sensing and GIS for surveillance of mosquito vector habitats and risk assessment. J Vector Ecol 23, 54-61.

Darsie RF, Ward RA, 1981. Identification and geographic distribution of mosquitoes of North America, north of Mexico, mosquito systematics supplement. Mosq Sys 1, 1-313.

Deutsch CV, Journal AG, 1992. Geostatistical Software Library and User's Guide, Oxford University Press, New York, USA.

Diuk-Wasser MA, Dolo G, Bagayoko M, Sogoba N, Toure MB, Moghaddam M, Manoukis N, Rian S, Traore SF, Taylor CE, 2006. Patterns of irrigated rice growth and malaria vector breeding in Mali using multi-temporal ERS-1 synthetic aperture radar. Int J Remote Sens 27, 535-548.

Dohm DJ, O'Guinn ML, Turell MJ, 2002. Effect of incubation at environmental temperature on the ability of *Culex pipiens* (Diptera: Culicidae) to transmit West Nile virus. J Med Entomol 39, 221-225.

Eidson M, Miller J, Kramer L, Cherry B, Hagiwara Y, 2001. Dead crow densities and human cases of West Nile virus, New York state, 2000. Emerg Infect Dis 7, 662-664.

Epstein PR, Defilippo C, 2001. West Nile virus and drought. Global Change Health 2, 105-107.

Gao J, Lo CP, 1995. Micro-scale modelling of terrain susceptibility to landsliding from a DEM: a GIS approach. Geocarto Int 10, 15-30.

Giles PT, Franklin SE, 1996. Comparison of derivative topographic surfaces of a DEM generated from stereoscopic SPOT images with field measurements. Photogramm Eng Rem S 62, 1165-1171.

Griffith DA, 2005. A comparison of six analytical disease mapping techniques as applied to West Nile Virus in the coterminous United States. Int J Health Geog 2, 4-18.

Gu W, Lampman R, Krosavin N, Berry R, Novak R, 2006. Spatio-temporal analyses of West Nile virus transmission in *Culex* mosquitoes in northern Illinois, USA. Vector Borne Zoonotic Dis 6, 91-98.

Gu W, Lampman R, Novak R, 2003. Problems in estimating mosquito infection rates using minimum infection rates. J Med Entomol 40, 595-596.

Gu W, Lampman R, Novak RJ, 2004. Assessment of arbovirus vector infection rates using variable size pooling. Med Vet Entomol 18, 200-204.

Gu W, Novak RJ, 2005. Habitat-based modeling of impacts of mosquito larval interventions on entomological inoculation rates, incidence, and prevalence of malaria. Am J Trop Med Hyg 73, 546-552.

Gu W, Unnasch TR, Katholi CR, Lampman R, Novak RJ, 2008. Fundamental issues in mosquito surveillance for arboviral transmission. Trans R Soc Trop Med Hyg 102, 817-822.

Hay SI, Omumbo JA, Craig MH, Snow RW, 2000. Earth observation, geographic information systems and *Plasmodium falciparum* malaria in sub-Saharan Africa. Adv Parasitol 47, 173-215.

Hay SI, Snow W, Rogers DJ, 1998. From predicting mosqui-

to habitat to malaria seasons using remotely sensed data: practice, problems and perspectives. Parasitol Today 14, 306-313.

Hayes EB, Komar N, Nasci RS, Montgomery SP, O'Leary DR, Campbell GL, 2005. Epidemiology and transmission dynamics of West Nile virus disease. Emerg Infect Dis 11, 1167-1173.

Huete AR, 1988. A soil adjusted vegetation index (SAVI). Remote Sens Environ 25, 295-309.

Huete AR, Hua G, Qi J, Chehbouni A, van Leeuwen WJD, 1992. Normalization of multidirectional red and NIR reflectances with the SAVI. Remote Sens Environ 41, 143-154.

Huete AR, Justice C, Liu H, 1994. Development of vegetation and soil indices for MODIS-EOS. Remote Sens Environ 49, 224-234.

Jackson RD, Huete AR, 1991. Intrepreting vegetation indices. Prev Vet Med 11, 185-167.

Jacob BG, Lampman RL, Ward MP, Muturi E, Funes J, Morris JC, 2009. Geospatial variability of *Culex pipiens* and *Culex restuans* aquatic habitats in urban Champaign, Illinois. Int J Remote Sens (in press).

Joy JE, Sullivan SN, 2005. Occurrence of tire inability mosquito larvae in different geographic regions of West Virginia. J Am Mosq Control Assoc 21, 380-386.

Kaufman YJ, Tanre D, 1992. Atmospheric resistant vegetation index (ARVI) for EOS-MODIS. IEEE. Trans Geo Remote Sensing 30, 261-270.

Kitron U, 1998. Landscape ecology and epidemiology of vector-borne disease: tools for spatial analysis. J Med Entomol 35, 435-445.

Kleinschmidt I, Sharp BL, Clarke CPY, Curtis B, Fraser C, 2001. Use of generalized linear mixed models in the spatial analysis of small-area malaria incidence rates in KwaZulu Natal, South Africa. Am J Epidemiol 153, 1213-1221.

Krige DG, 1966. Two dimensional weighted moving average trend surfaces for ore-evaluation. J S African Inst Minning Metallurgy 66, 13-38.

Kulldroff M, 1997. A spatial scan statistic. Comm Stats Theory Methods 26, 1481-1496.

Kunkel KE, Novak R, 2005. Climate index for West Nile Virus. Am Meteorol Soc B 86, 18.

Kutz FW, Wade TG, Pagac BB, 2003. A geospatial study of the potential of two exotic species of mosquitoes to impact the epidemiology of West Nile virus in Maryland. J Am Mosq Control Assoc 19, 190-198.

Lacaux JP, Tourre YM, Vignolles C, Ndione JA, Lafaye M, 2006. Classification of ponds from high resolution remote sensing: application to Rift Valley fever epidemics in Senegal. Remote Sensing Environ 15, 66-74.

Lampman RL, Novak RJ, 1996. Oviposition preferences of *Culex pipiens* and *Culex restuans* for infusion-baited traps. J Am Mosq Control Assoc 12, 23-32.

Lampman RL, Slamecka M, Krasavin N, Kunkel K, Novak R, 2006. *Culex* population dynamics and West Nile virus transmission in east-central Illinois. J Am Mosq Control Assoc 22, 390-400.

Landesman WJ, Allan BF, Langerhans RB, Knight TM, Chase JM, 2007. Inter-annal associations between precipitation and human incidence of West Nile Virus in the United States. Vector Borne Zoonotic Dis 7, 337-343.

Linthicum KI, Bailey CL, Davies FG, Tucker CJ, 1987. Detection of Rift Valley fever viral activity in Kenya by satellite remote sensing imagery. Science 235, 1656-1659.

Lopes P, Lourenco P, Sousa C, Novo T, Rodrigues A, Almeida PG, Seixas J, 2005. Modeling patterns of mosquito density based on remote sensing images. In: Proceedings of the II International Conference and Exhibition on Geographic Information, Estoril, Portugal, May 30-June 2, 2005.

Magurran AE, 1988. Ecological diversity and its measurement. Chapman and Hall, London, UK.

May RM, 1981. Theoretical ecology. Principles and applications. WB Saunders Company, Philadelphia, PA, USA.

Meece JK, Henkel JS, Glaser L, Reed KD, 2003. Mosquito surveillance for West Nile virus in southeastern Wisconsin-2002. Clin Med Res 1, 37-42.

Mushinzimana E, Munga S, Minakawa N, Li L, Feng C, Bian L, Kitron U, Schmidt C, Beck L, Zhou G, Githeko AK, Yan G, 2006. Landscape determinants and remote sensing of anopheline mosquito larval habitats in the western Kenya highlands. Mal J 5, 13.

Nicholson MC, Mather TN, 1996. Methods for evaluating Lyme disease risks using geographic information systems and geospatial analysis. J Med Entomol 33, 711-720.

Pampana EJ, 1969. Textbook of Malaria Eradication, 2nd edn. Oxford University Press, 608 pp.

Pan American Health Organization, 2000. Epidemiological Calendar 2001. Epidemiol Bull 21, 15.

Patz JA, Martens WJM, Focks DA, Jetten TH, 1998. Dengue

fever epidemic potential as projected by general circulation models of global climate change. Environ Health Perspec 106, 147-153.

Petersen LR, Marfin AA, Gubler DJ, 2003. West Nile virus. J Am Med Assoc 290, 524-528.

Pierce LL, Running SW, 1988. Rapid estimation of coniferous forest leaf area index using a portable integration. Ecology 69, 1762-1767.

Pierce LL, Running SW, Walker J, 1994. Regional-scale relationships of leaf area index to specific leaf area and leaf nitrogen content. Ecol Appl 4, 313-321.

Ramachandra Rao T, 1984. *Anopheles* of India. Malaria Research Centre, Indian Council of Medical Research.

Reisen W, Lothrop H, Chiles R, Madon M, Cossen C, Woods L, Husled S, Kramer V, Edman J, 2004. West Nile virus in California. Emerg Infect Dis 10, 1369-1378.

Rogers DJ, Randolph SE, Snow RW, Hay SI, 2002. Satellite imagery in the study and forecast of malaria. Nature 415, 710-715.

Ruiz MO, Tedesco C, McTighe TJ, Austin C, Kitron U, 2004. Environmental and social determinants of human risk during a West Nile virus outbreak in the greater Chicago area, 2002. Int J Health Geog 3, 8.

Service MW, 1976. Mosquito ecology-field sampling methods. Halstead Press, John Wiley and Sons, Inc, New York, USA, 954 pp.

Shaman J, Stieglitz M, Stark C, Le Blancq S, Cane M, 2002. Using a dynamic hydrology model to predict mosquito abundances in flood and swamp water. Emerg Infect Dis 8, 6-13.

Sithiprasasna R, Lee WJ, Ugsang DM, 2005. Identification and characterization of larval and adult anopheline mosquito habitats in the Republic of Korea: potential use of remotely sensed data to estimate mosquito distributions. Int J Health Geogr, 4.

Srivastava A, Nagpal B, Saxena R, Subbarao S, 2001. Predictive habitat modeling for forest malaria vector species *An. dirus* in India- a GIS based approach. Current Sci 80, 1129-1134.

Theophilides CN, Ahearn SC, Binkowski ES, Paul WS, Gibbs K, 2006. First evidence of West Nile virus amplification and relationship to human infections. Int J Geograph Info Sci 20, 103-115.

Tucker CJ, 1979. Red and photographic infrared linear combinations for monitoring vegetation. Remote Sens Environ 8, 127.

Ward MP, Levy M, Thacker HL, Ash M, Norman SKL, Moore GE, Webb PW, 2004. An outbreak of West Nile virus encephalomyelitis in a population of Indiana horses: 136 cases. Am Vet Med Assoc 222, 84-89.

Wittich CA, Ward MP, Fosgate GT, Srinivasan R, 2008. Identification of hyperendemic foci of horses with West Nile virus disease in Texas. Am J Vet Res 79, 378-384.